Acta Crystallographica Section F
Structural Biology and Crystallization Communications
ISSN 1744-3091

An improved resolution structure of the human β common receptor involved in IL-3, IL-5 and GM-CSF signalling which gives better definition of the high-affinity binding epitope

P. D. Carr,[a]* F. Conlan,[b] S. Ford,[b] D. L. Ollis[a] and I. G. Young[b]

[a]Research School of Chemistry, Australian National University, Canberra, Australia, and [b]John Curtin School of Medical Research, Australian National University, Canberra, Australia

Correspondence e-mail: pdc@rsc.anu.edu.au

Received 1 March 2006
Accepted 8 May 2006

PDB Reference: human β common receptor, 2gys.

X-ray diffraction has been used to produce and refine a model of the extracellular domains of the β common cytokine receptor. A minor improvement in resolution has resulted in improved electron-density maps, which have given a clearer indication of the position and stabilization of the key residues Tyr15, Phe79, Tyr347, His349, Ile350 and Tyr403 in the elbow region between domain 1 and domain 4 of the dimer-related molecule.

1. Introduction

Granulocyte/macrophage-colony stimulating factor (GM-CSF), interleukin-3 (IL-3) and interleukin-5 (IL-5) are cytokines produced by activated T-cells during immune responses to infections. They have overlapping activities on haematopoietic cells and have been implicated in the pathogenesis of allergic diseases of the lung such as asthma (Foster *et al.*, 1996; Mould *et al.*, 1997). They are also believed to be centrally involved in other chronic inflammatory diseases such as arthritis and multiple sclerosis (Cook *et al.*, 2001; McQualter *et al.*, 2001). All three cytokines signal across membranes *via* the common β receptor (βc) in complexes containing the cytokine ligands (GM-CSF, IL-3 or IL-5), a cytokine-specific α receptor (GMCSFα, IL3α, IL5α) and βc. Janus kinases (JAKs) that are constitutively associated with the receptor cytoplasmic domains are able to transactivate one another and initiate signalling. The signalling pathways initiated in this manner include the Ras/MAPK, PI3K and JAK/STAT pathways (reviewed by de Groot *et al.*, 1998).

We have previously reported the structure of the extracellular domain of the unliganded βc molecule at a resolution of 3.0 Å (Carr *et al.*, 2001). The structure revealed a novel intertwined dimer (Fig. 1) and suggested a potential ligand-binding site at the elbow region between domain 1 (*AB* and *EF* loops) and domain 4 (*BC* and *FG* loops) of the dimer-related chain. Mutagenesis studies have

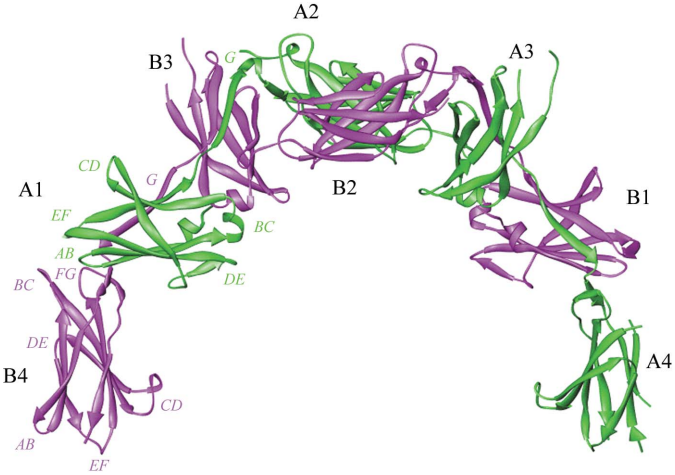

Figure 1
Overall topology of the βc dimer. One monomer is shown in green and the other in magenta. Black labels indicate domain names; green and magenta labels indicate loops and the *G* strands of domains *A*1 and *B*4, respectively.

Table 1
Data collection and processing.

(*a*) Data-collection statistics.

Space group	*R*3 (hexagonal setting)
Unit-cell parameters (Å)	a = 184.9, c = 101.0
No. of observed reflections	192931
No. of unique reflections	32327
$\langle I/\sigma(I)\rangle$	13.2

(*b*) Statistics in resolution shells.

Resolution	N_{res}	Intensity	$I/\sigma(I)$	R_{merge}†	Completeness (%)
50.0–5.81	3528	23574	48.2	0.054	99.9
5.81–4.62	3552	18620	41.9	0.053	100.0
4.62–4.03	3539	16267	30.2	0.053	100.0
4.03–3.66	3554	10072	22.5	0.065	100.0
3.66–3.40	3506	7698	17.8	0.072	100.0
3.40–3.20	3546	5280	13.6	0.086	100.0
3.20–3.04	3539	3031	7.9	0.110	100.0
3.04–2.91	3435	1779	4.4	0.142	96.5
2.91–2.80	2697	1305	2.7	0.148	77.2
2.80–2.70	1431	1094	2.4	0.153	40.2
All	32327	9599	19.2	0.060	91.4

† $R_{merge} = \sum_{hkl} |I_{hkl} - \langle I_{hkl}\rangle| / \sum_{hkl} I_{hkl}$.

confirmed the importance of domains 1 and 4 in high-affinity binding (Murphy *et al.*, 2003, 2004), indicating the existence of a functional epitope formed between domains 1 and 4 of the two different protein chains.

The current study describes the structure of the same extracellular domains refined using data to a maximum resolution of 2.7 Å. Although this is a modest increase in resolution, it produced electron-density maps of greater clarity and resolved the carbonyl oxygen positions of most peptide residues, allowing us to confidently assign dihedral angles. The critical residues in the elbow region now have unequivocal density associated with them, which reveals a clustering of the hydrophobic parts of their side chains and a more compact functional epitope than previously suggested. We postulate that the hydrophobic interactions hold an inherently labile region in the conformation required for high-affinity binding and subsequent signalling.

2. Materials and methods

2.1. Protein expression, purification and crystallization

Full details of the protein expression, purification and crystallization are given in Gustin *et al.* (2001). Briefly, the extracellular domain of human βc was expressed in insect cells, concentrated by ultrafiltration and purified by gel-filtration and anion-exchange chromatography. Crystals were obtained from sitting drops using well buffers containing 7–10% polyethylene glycol 5000 monomethyl ether in phosphate buffer pH 6.2–6.6 at 277 K. A cryoprotectant similar to the crystallization buffer but containing 20% 2-methyl-2,4-pentanediol was used when flash-cooling the crystals to 100 K. These conditions are the same as previously reported.

2.2. Data collection and processing

A number of crystals were screened on beamline ID14B at BioCARS, Advanced Photon Source, Chicago, USA. The wavelength used was 1.117 Å. Once the crystal that diffracted to the best resolution had been identified, two data-collection passes were made. The first consisted of 180 × 1° oscillations of 60 s each. This pass optimized the intensity of the weaker reflections in the highest resolution shells, but caused some spots at lower resolution to saturate the detector. A second pass was made consisting of 180 × 1° oscillations of 10 s. The intensities of the low-angle spots from the second pass were within the dynamic range of the detector and were therefore accurately determined. Data processing, reduction and scaling were performed using *DENZO* and *SCALEPACK* (Otwinowski & Minor, 1997). The data-collection parameters and scaling statistics are listed in Table 1.

Table 2
Refinement statistics.

Residues omitted from the final model: *A*133–137, *A*258–262, *A*331–333, *A*343–350, *B*133–137 and *B*260–266. Residues truncated to C^{β} labelled as alanines in the final model: *A*1, 31, 78, 122, 125, 141, 159, 197, 199, 255, 257, 264, 265, 266, 276, 281, 294, 304, 316, 334, 335, 337, 341, 342, 360, 366, 368, 369, 375, 388, 389, 415, 417, 418 and *B* 1, 16, 41, 43, 45, 46, 50, 90, 101, 157, 159, 160, 196, 259, 267, 326, 331, 332, 334, 336, 337, 343, 344, 360, 366, 369, 371, 381, 385, 387, 415.

Resolution limits (Å)	50.0–2.7
No. of reflections in working set	30934
No. of reflections in test set	1392 (4.3%)
R (test and working sets)	0.214
R (working set)	0.212
R_{free}	0.269
No. of atoms refined	
Protein	6278
Carbohydrate	172
Temperature factors (Å^2)	
Overall B	51.11
$B11$	−1.16
$B22$	−1.16
$B33$	1.74
$B12$	−0.58
$B13$	0.00
$B23$	0.00
Cruickshank's DPI (Å)	0.34
Overall figure of merit	0.77
Deviations from ideal geometry	
R.m.s. bond length (Å)	0.022
R.m.s. bond angle (°)	2.217
TLS parameters	
Group a1	
Range	*A*1–91, *B*310–317
T	−0.219 −0.294 −0.143 −0.043 −0.014 −0.017
L	8.984 1.173 2.35 −1.094 0.707 −0.091
S	−0.063 −0.278 0.4877 −0.422 0.115 0.027 0.277
Group a2	
Range	*A*106–215
T	−0.110 −0.193 −0.0987−0.028 −0.003 0.079
L	1.3964.713 5.159 1.326 1.978 3.442
S	0.214 0.214 −0.022 −0.148 −0.013 0.228 −0.175 0.424
Group a3	
Range	*A*220–300, *B*94–103
T	0.041 −0.039 0.1331 −0.113 −0.171 0.006
L	2.1857 4.814 8.105 −2.728 −4.174 4.778
S	−0.288 0.651 −0.002 0.242 −0.353 0.240 0.111 0.527
Group a4	
Range	*A*320–418
T	0.403 0.137 0.335 −0.004 0.149 −0.016
L	1.2039 8.0014 4.830 −2.625 −1.969 2.376
S	−0.187 0.644 0.414 0.588 0.786 0.207 −0.579 −0.662
Group b1	
Range	*B*1–91, *A*310–317
T	0.076 0.078 −0.138 −0.077 0.0266 −0.0488
L	1.258 9.59 3.18 0.327 −0.306 −0.394
S	0.024 −0.035 −0.232 −0.1333 −0.223 0.864 0.269 −0.029
Group b2	
Range	*B*106–215
T	−0.287 −0.295 0.001 0.001 0.068 −0.043
L	6.987 0.963 7.839 0.069 5.199 0.064
S	−0.122 0.298 −0.330 0.058 −0.247 0.418 −0.070
Group b3	
Range	*B*220–307, *A*94–103
T	−0.335 −0.247 −0.046 −0.000 −0.027 −0.006
L	1.612 6.089 5.497 −1.245 1.557 −5.728
S	−0.1336 0.231 0.081 −0.1828 0.202 0.231 0.0234 0.015
Group b4	
Range	*B*320–418
T	0.058 −0.058 0.019 0.089 −0.137 0.011
L	4.086 4.519 4.120 −0.477 1.036 −2.284
S	0.251 −0.144 0.649 0.669 0.286 −0.151 −0.934 −0.468

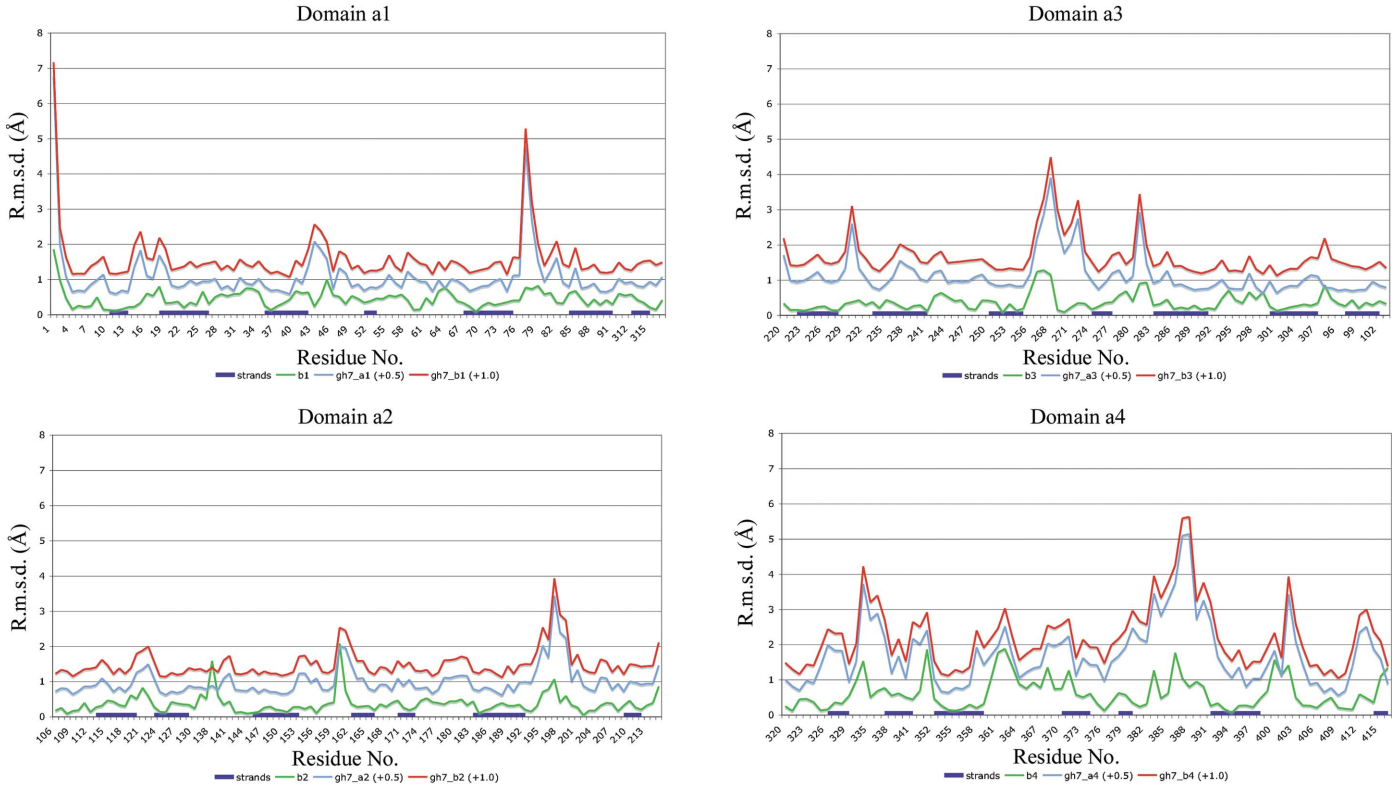

Figure 2
Graphs showing r.m.s. displacements in Å of main-chain atoms when individual domains are overlaid. The program *LSQKAB* (Kabsch, 1976) was used to calculate the displacements. Domains are compared with the dimer-related domain from the current study (labelled b1, b2, b3 and b4), in addition to both the equivalent and dimer-related domains in the previous study. The prefix gh7 indicates the comparison is for domains from 1gh7. Multiple plots have been displaced by 0.5 Å vertically on each graph to aid clarity. A blue bar on the residue-number axis indicates the position of β-strands.

2.3. Refinement

Initial rigid-body refinements and subsequent restrained refinements were performed using *REFMAC* 5.2.0019 (Murshudov *et al.*, 1997) as implemented in *CCP*4 (Collaborative Computational Project, Number 4, 1994). All data were used in the refinement, with the exception of 1392 reflections (4.3%) flagged for cross-validation purposes. No sigma cutoff was applied. PDB entry 1gh7 was used as an initial model. Each of the fibronectin domains, eight in total, was treated as a separate group for TLS refinement (Winn *et al.*, 2001). Table 2 shows the final TLS parameters along with other refinement statistics. Cycles of TLS and restrained refinements (with individual *B*-factor refining) were interspersed with manual rebuilding of the model using *COOT* (Emsley & Cowtan, 2004). Areas flagged by *COOT* as having poor geometry or density fit were rebuilt into OMIT maps (Bhat, 1988). Table 2 lists regions of the model omitted owing to poor density.

3. Results

3.1. Quality of the model

The final model had R_{work} and R_{free} values of 0.212 and 0.269, respectively, which compare favourably with those obtained in the 1gh7 study (0.267/0.304). Table 2 lists the full refinement statistics and associated stereochemical residuals. The stereochemistry of the final model was checked using the programs *PROCHECK* (Laskowski *et al.*, 1993), *WHATCHECK* (Hooft *et al.*, 1996) and *SFCHECK*

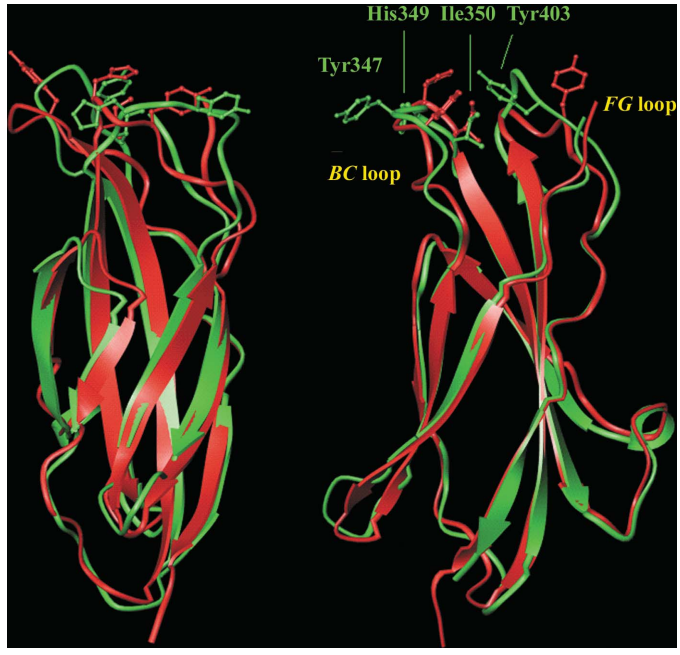

Figure 3
Orthogonal views of the overlay of domain 4 from 1egj (Rossjohn *et al.*, 2000; red) and the current study (green). Residues implicated by mutagenesis as important in affinity conversion are shown in ball-and-stick representation (His349, Tyr347, Ile350 and Tyr403).

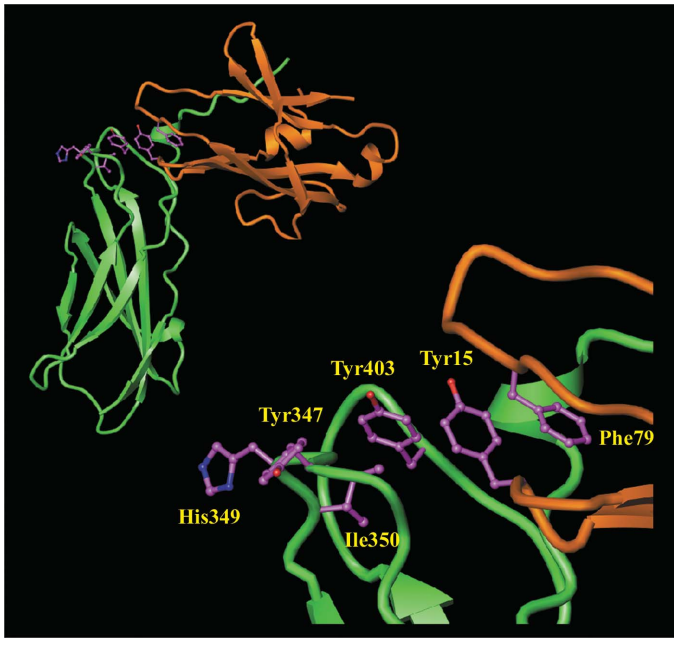

Figure 4
Domains *A*1/*B*4 from the current study, showing the position of the residues involved in high-affinity complex formation.

(Vaguine *et al.*, 1999). 98.7% of residues fall into the most favoured or additionally allowed regions, 0.7% into generously allowed regions and 0.6% into disallowed regions on a Ramachandran plot. Both main-chain and side-chain parameters were flagged as being within normal limits or better, with an overall *G* factor of −0.3 from *PROCHECK*.

3.2. Description of the model

The overall topology of the interlocking fibronectin domains is the same as reported previously (Carr *et al.*, 2001; Fig. 1). Fig. 2 shows graphs of the r.m.s. deviation of backbone atoms when overlaid with the dimer-related molecule or the originally reported structure 1gh7. From these graphs, it is evident that the regions of maximal variation occur at the loop regions connecting β-strands of the fibronectin domains. Domain 4 shows the largest displacements; it also has large TLS parameters (Table 2). This indicates that this domain is mobile with respect to the rest of the structure. Domain 4 was the most poorly defined domain in the previously reported structure. Given that this domain is tethered to the membrane *in vivo via* the membrane-spanning portion of the protein chain, it is perhaps not surprising that it is the most mobile when the extracellular domain is crystallized from solution.

A crystal structure of domain 4 determined in complex with an antibody Fab fragment is available (Rossjohn *et al.*, 2000; PDB code 1egj). Fig. 3 shows an overlay of this structural model, without the Fab fragment, onto domain B4 of the current study. The β-strands overlay closely, but the membrane-distal loops *BC* and *FG* show distinctly different conformations. These differences may result partly from interactions with the Fab fragment and partly from the absence of interacting residues from domain 1 (see below). Mutational studies have implicated a number of residues in the elbow region between domain 1 and domain 4 of the dimer-related chain as important for affinity conversion and subsequent signalling events. These residues are Tyr15, Phe79 (Murphy *et al.*, 2003), His349 (Lock *et al.*, 1994; Woodcock *et al.*, 1994), Tyr347, Ile350 (Woodcock *et al.*, 1994) and Tyr403 (Woodcock *et al.*, 1996). Fig. 4 shows the location of these residues in the current model. They form an extended hydrophobic network suggestive of a role in orienting the inherently labile loops in this region into a position suitable for complex formation with the low-affinity complex of a cytokine ligand and its cognate α receptor. The residues comprising the functional epitope in the isolated domain 4 structure and in our previous structure of the complete extracellular domain appeared to be much less compact than those of other class I cytokine receptors. However, the present structure indicates a more compact functional epitope. In particular, Tyr403, the side-chain position of which was ambiguous in 1gh7, is now better integrated with the other functional residues (Figs. 4 and 5).

Of the residues implicated in affinity conversion by mutagenesis, Tyr347 and His349 exhibit good surface accessibilities of 228 and 122 Å^2, respectively. The surface accessibilities of Tyr15, Phe79, Ile350 and Tyr403 are much lower (0, 14, 13 and 33 Å^2, respectively), which would indicate a structural role. However, the mutation Y403F has been shown to abolish binding (Murphy *et al.*, 2003), which indicates that the hydroxyl moiety must be important. Fig. 6 shows the surface topology, colour coded by the electrostatic potential of the underlying charged residues, in the elbow region. It can be seen that the exposed residues protrude in a manner that makes them available for direct interactions with other molecules involved in the signalling process and that some of the residues forming the hydrophobic network stabilizing the loops in this region also point towards charged patches on the concave surface immediately behind residues Tyr347 and His349. The residue Arg400, which is well defined in the current study, but not in the 1gh7 structure, appears to delimit the hydrophobic cluster of residues Phe79, Tyr15, Tyr403 and Ile350 with the aliphatic part of the side chain. Its guanidino group points towards His349, contributing to the local surface charge. Arg400 was not, however, indicated as an essential residue by mutagenesis (Woodcock *et al.*, 1996). The program *LIGPLOT* (Wallace *et al.*, 1995) was used to identify hydrophobic contacts. The program uses a cutoff of 3.9 Å to define contacts. Using this criterion, Phe79 directly contacts Tyr15, whereas Tyr15 indirectly contacts Tyr403

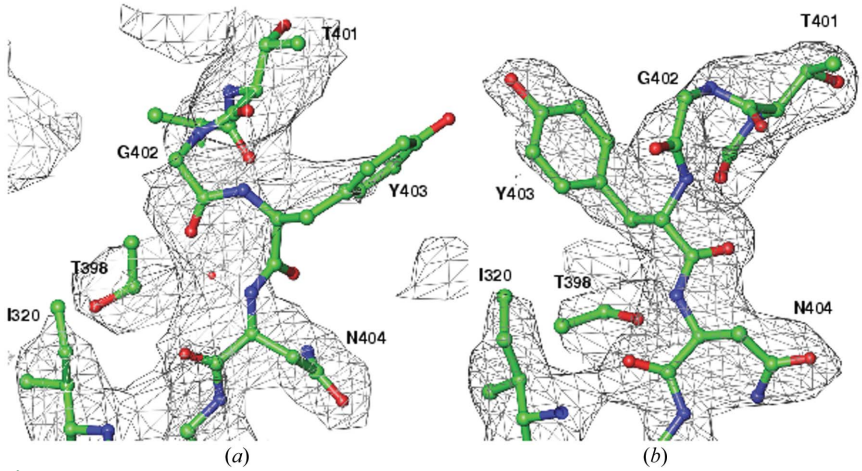

Figure 5
$2m|F_o| - D|F_c|$ electron-density maps, contoured at 1σ, of the final models from (*a*) the original 3.0 Å resolution study and (*b*) the current study.

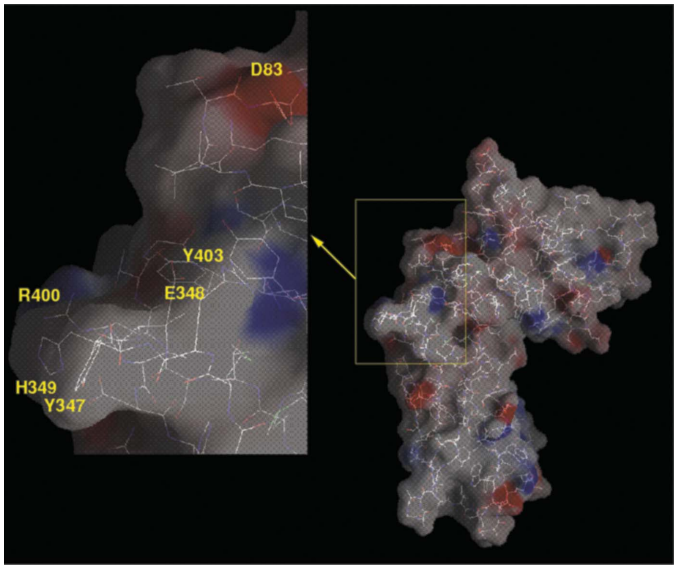

Figure 6
GRASP surface plot of the elbow region showing the position of surface-exposed and charged residues. The electrostatic potential at the surface of fully charged side chains are indicated with blue (positive) and red (negative) colours. Charge assignments were made using the full.crg file supplied with the program; lysine NZ atoms +1.0 e, arginine NH1, NH2 +0.5 e, glutamic acid OE1, OE2 −0.5 e and aspartate OD1, OD2 −0.5 e.

via Ile320. Tyr403 makes a direct contact to Ile350 and a further indirect contact to His349 *via* Arg400. The latter contact was at a distance of 4.05 Å, slightly longer than the program's default value but still reasonable for a hydrophobic effect.

4. Discussion

The current structure, although largely similar to the previously reported 1gh7 (Carr *et al.*, 2001), is determined from electron-density maps of superior quality (Fig. 5). In particular, the model in the region of the functionally important elbow region now indicates that key residues of the functional epitope exist in a more compact cluster than previous structures suggested. The residues implicated by mutagenesis studies fall into two groups based on their surface accessibility. The residues in one group (Tyr15, Phe79, Ile350 and Tyr403) have little surface accessibility and appear to maintain an inherently labile region in a conformation suitable for complex formation. In contrast, the other more exposed residues (His349 and Tyr347) probably engage the low-affinity complex between the cytokine and its cognate α-receptor directly. There is some evidence that the surface charge on the region above the stabilized loops is also important in complex formation. Clarification of whether or not the buried residues of the functional epitope are re-oriented in the high-affinity complex to engage with ligand awaits the determination of a structure of the complex.

Harry Tong and the staff at BioCARS are warmly thanked for their assistance during data collection. The ASRP is thanked for funding for travel and subsistence. This work is supported in part by a grant from the National Health and Medical Research Council of Australia.

References

Bhat, T. N. (1988). *J. Appl. Cryst.* **21**, 279–281.
Carr, P. D., Gustin, S. E., Church, A. P., Murphy, J. M., Ford, S. C., Mann, D. A., Woltring, D. M., Walker, I., Ollis, D. L. & Young, I. G. (2001). *Cell*, **104**, 291–300.
Collaborative Computational Project, Number 4 (1994). *Acta Cryst.* D**50**, 760–763.
Cook, A. D., Braine, E. L., Campbell, I. K., Rich, M. J. & Hamilton, J. A. (2001). *Arthritis Res.* **3**, 293–298.
Emsley, P. & Cowtan, K. (2004). *Acta Cryst.* D**60**, 2126–2132.
Foster, P. S., Hogan, S. P., Ramsay, A. J., Matthaei, K. I. & Young, I. G. (1996). *J. Exp. Med.* **183**, 195–201.
de Groot, R. P., Coffer, P. J. & Koenderman, L. (1998). *Cell. Signal.* **10**, 619–628.
Gustin, S. E., Church, A. P., Ford, S. C., Mann, D. A., Carr, P. D., Ollis, D. L. & Young, I. G. (2001). *Eur. J. Biochem.* **268**, 2905–2911.
Hooft, R. W. W., Vriend, G., Sander, C. & Abola, E. E. (1996). *Nature (London)*, **381**, 272.
Kabsch, W. (1976). *Acta Cryst.* A**32**, 922–923.
Laskowski, R. A., MacArthur, M. W., Moss, D. W. & Thornton, J. M. (1993). *J. Appl. Cryst.* **26**, 283–291.
Lock, P., Metcalf, D. & Nicola, N. A. (1994). *Proc. Natl Acad. Sci. USA*, **91**, 252–256.
McQualter, J. L., Darwiche, R., Ewing, C., Onuki, M., Kay, T. W., Hamilton, J. A., Reid, H. H. & Bernard, C. C. A. (2001). *J. Exp. Med.* **194**, 873–881.
Mould, A. W., Matthaei, K. I., Young, I. G. & Foster, P. S. (1997). *J. Clin. Invest.* **99**, 1064–1071.
Murphy, J. M., Ford, S. C., Olsen, J. E., Gustin, S. E., Jeffrey, P. D., Ollis, D. L. & Young, I. G. (2004). *J. Biol. Chem.* **279**, 26500–26508.
Murphy, J. M., Ford, S. C., Wiedemann, U. A., Carr, P. D., Ollis, D. L. & Young, I. G. (2003). *J. Biol. Chem.* **278**, 10572–10577.
Murshudov, G. N., Vagin, A. A. & Dodson, E. J. (1997). *Acta Cryst.* D**53**, 240–255.
Otwinowski, Z. & Minor, W. (1997). *Methods Enzymol.* **276**, 307–326.
Rossjohn, J., McKinstry, W. J., Woodcock, J. M., McClure, B. J., Hercus, T. R., Parker, M. W., Lopez, A. F. & Bagley, C. J. (2000). *Blood*, **95**, 2491–2498.
Vaguine, A. A., Richelle, J. & Wodak, S. J. (1999). *Acta Cryst.* D**55**, 191–205.
Wallace, A. C., Laskowski, R. A. & Thornton, J. M. (1995). *Protein Eng.* **8**, 127–134.
Winn, M. D., Isupov, M. N. & Murshudov, G. N. (2001). *Acta Cryst.* D**57**, 122–133.
Woodcock, J. M., Bagley, C. J., Zacharakis, B. & Lopez, A. F. (1996). *J. Biol. Chem.* **271**, 25999–26006.
Woodcock, J. M., Zacharakis, B., Plaetinck, G., Bagley, C. J., Qiyu, S., Hercus, T. R. & Lopez, A. F. (1994). *EMBO J.* **13**, 5176–5185.